

# Scaling DoRA: High-Rank Adaptation via Factored Norms and Fused Kernels

Alexandra Zelenin\*      Alexandra Zhuravlyova

March 24, 2026

## Abstract

Weight-Decomposed Low-Rank Adaptation (DoRA; Liu et al. [2024]) extends LoRA by decoupling weight magnitude from direction, but its forward pass requires the row-wise norm  $\|\mathbf{W} + s\mathbf{BA}\|_{\text{row}}$ , a computation that every major framework we surveyed implements by materializing the dense  $[d_{\text{out}}, d_{\text{in}}]$  product  $\mathbf{BA}$ . At  $d_{\text{in}} = 8192$  and rank  $r = 384$ , a single module’s norm requires  $\sim 512$  MB of transient working memory in bf16, making high-rank DoRA costly and often infeasible on common single-GPU setups once hundreds of adapted modules and checkpointing are involved.

We present two systems contributions: a *factored norm* that decomposes the squared norm into base, cross, and Gram terms computable through  $\mathcal{O}(d_{\text{out}}r + r^2)$  intermediates, eliminating the dense product. *Fused Triton kernels* collapse the four-kernel DoRA composition into a single pass, reducing memory traffic by  $\sim 4\times$  and using a numerically stable form that avoids catastrophic cancellation in the near-unity rescaling regime where magnitude scales concentrate in practice.

Across six 8–32B vision-language models (VLMs) on three NVIDIA GPUs (RTX 6000 PRO, H200, B200) at  $r = 384$  in bf16, the fused implementation is 1.5–2.0 $\times$  faster than HF PEFT’s DoRA implementation for inference, and 1.5–1.9 $\times$  faster for gradient computation (optimizer step excluded), with up to 7 GB lower peak VRAM. Microbenchmarks on six GPUs spanning four architecture generations (L40S, A100, RTX 6000 PRO, H200, B200, B300) confirm 1.5–2.7 $\times$  compose-kernel speedup. Final-logit cosine similarity exceeds 0.9999 across all model/GPU pairs, and multi-seed training curves match within  $7.1 \times 10^{-4}$  mean per-step loss delta over 2000 steps.

## 1 Introduction

Low-Rank Adaptation (LoRA; Hu et al. 2022) is the dominant method for parameter-efficient fine-tuning. DoRA [Liu et al., 2024] extends LoRA by decomposing the adapted weight into magnitude and direction:

$$\mathbf{W}' = \mathbf{m} \odot \frac{\mathbf{W} + s\mathbf{BA}}{\|\mathbf{W} + s\mathbf{BA}\|_{\text{row}}} \quad (1)$$

where  $\mathbf{W} \in \mathbb{R}^{d_{\text{out}} \times d_{\text{in}}}$  is the frozen base weight,  $\mathbf{B} \in \mathbb{R}^{d_{\text{out}} \times r}$  and  $\mathbf{A} \in \mathbb{R}^{r \times d_{\text{in}}}$  are low-rank factors,  $s$  is a scaling coefficient (e.g., rsLoRA; Kalajdzievski 2023), and  $\mathbf{m} \in \mathbb{R}^{d_{\text{out}}}$  is a learnable magnitude vector. High-rank configurations narrow the gap to full fine-tuning on complex downstream tasks [Hu et al., 2022, Liu et al., 2024]. We treat weights as  $[d_{\text{out}}, d_{\text{in}}]$  and compute per-output-row norms ( $\text{dim}=1$ ), consistent with PEFT and torchtune.

---

\*Correspondence: alexa@eyes.ml

The bottleneck is the row-wise  $L_2$  norm of the composed weight  $\mathbf{W} + s\mathbf{BA}$ . Hugging Face PEFT [Mangrulkar et al., 2022] (and five other major frameworks we surveyed: torchtune, Unsloth, SWIFT, LLaMA-Factory, Axolotl; see Appendix G) computes this by constructing a  $d_{\text{in}} \times d_{\text{in}}$  identity matrix, thereby materializing the dense product  $\mathbf{BA}$ :

```
x_eye = torch.eye(lora_A.weight.shape[1], ...) # [d_in, d_in]
lora_weight = lora_B(lora_A(x_eye)).T # [d_out, d_in]
weight_norm = torch.linalg.norm(weight + scaling * lora_weight, dim=1)
```

This incurs  $\mathcal{O}(d_{\text{in}}^2)$  memory for the identity matrix alone: 32 MB at  $d_{\text{in}} = 4096$ , 128 MB at  $d_{\text{in}} = 8192$  in bf16. Including the dense  $\mathbf{BA}$  product and composed-weight copy, a single module allocates 3–4 dense  $[d_{\text{out}}, d_{\text{in}}]$  temporaries:  $\sim 512$  MB at  $d_{\text{in}} = 8192$ . With gradient checkpointing [Chen et al., 2016], these temporaries are allocated *twice* per step. Across hundreds of adapted modules in an 8–32B model, this cumulative pressure is a major contributor to both speed degradation and OOM failures at high rank.

The most obvious fix (computing `lora_B.weight @ lora_A.weight` directly) eliminates the identity matrix but still materializes the full  $[d_{\text{out}}, d_{\text{in}}]$  product, which is the dominant cost. We show in §5.3 that this “dense (B@A)” path provides inconsistent speedups that depend on GPU bandwidth class and sometimes runs *slower* than the PEFT baseline.

This paper does not propose a new adapter architecture, optimizer, or training recipe. Our contribution is systems-oriented: we execute the same DoRA computation with a smaller working set and lower memory traffic. Specifically:

1. A **factored norm computation** (§2) decomposes  $\|\mathbf{W} + s\mathbf{BA}\|_{\text{row}}^2$  into three terms, each evaluable through  $\mathcal{O}(d_{\text{out}}r + r^2)$  intermediates without materializing  $\mathbf{BA}$ . At  $d = 8192$ ,  $r = 512$  in fp32, the theoretical persistent-memory reduction is  $15\times$  (Table 1).
2. **Fused Triton kernels** (§3) collapse the DoRA composition  $(g-1)\odot\text{base} + g\odot s\odot\text{lora}$  from four CUDA kernel launches to one pass. A numerically stable form avoids catastrophic cancellation when  $g \approx 1$ . Forward speedup:  $1.5\text{--}2.7\times$  (geometric mean); backward speedup:  $1.06\text{--}1.23\times$ . A three-tier runtime dispatch (§4) selects the optimal path (fused backward for training, fused forward for inference, eager fallback for CPU or sub-crossover shapes), compatible with `torch.compile` [Ansel et al., 2024], gradient checkpointing, DeepSpeed ZeRO [Rajbhandari et al., 2020], and FSDP1.

Both contributions are validated on six NVIDIA GPUs spanning four architecture generations (L40S, A100, RTX 6000 PRO, H200, B200, B300; 48–268 GB) with model-level benchmarks on three GPUs across six 8–32B VLMs (§5). Throughout this paper, four configurations are compared: *PEFT* (unmodified HF PEFT identity-matrix path), *Dense (B@A)* (direct product, still materializes the full matrix), *Eager* (our factored norm with PyTorch composition), and *Fused* (our factored norm with Triton kernels).

## 2 Factored Norm Computation

### 2.1 Algebraic Decomposition

The row-wise squared norm of the composed weight expands into three terms:

$$\|\mathbf{W} + s\mathbf{BA}\|_{\text{row}}^2 = \underbrace{\|\mathbf{W}\|_{\text{row}}^2}_{\text{base}} + \underbrace{2s\langle\mathbf{W}, \mathbf{BA}\rangle_{\text{row}}}_{\text{cross}} + \underbrace{s^2\|\mathbf{BA}\|_{\text{row}}^2}_{\text{BA norm}} \quad (2)$$

where  $\langle \cdot, \cdot \rangle_{\text{row}}$  denotes the row-wise inner product. Each term is computable through low-rank intermediates:

**Base norm.**  $\|\mathbf{W}\|_{\text{row}}^2$  accumulates via chunks along  $d_{\text{in}}$ , producing a vector of size  $d_{\text{out}}$ . Chunking limits working memory to a configurable budget (default: 256 MB).

**Cross term.** The row-wise inner product rewrites as:

$$\langle \mathbf{W}, \mathbf{BA} \rangle_j = \sum_{\ell} B_{j\ell} \cdot U_{j\ell} = (\mathbf{B} \odot \mathbf{U})_j \cdot \mathbf{1} \quad (3)$$

where  $\mathbf{U} = \mathbf{WA}^\top \in \mathbb{R}^{d_{\text{out}} \times r}$  accumulates chunk-wise:  $\mathbf{U} \leftarrow \mathbf{U} + \mathbf{W}_c \mathbf{A}_c^\top$ .

**BA norm.** The row-wise squared norm factors through the Gram matrix:

$$\|\mathbf{BA}\|_j^2 = (\mathbf{BG} \odot \mathbf{B})_j \cdot \mathbf{1} \quad (4)$$

where  $\mathbf{G} = \mathbf{AA}^\top \in \mathbb{R}^{r \times r}$  also accumulates chunk-wise. At  $r = 512$  in fp32,  $\mathbf{G}$  occupies 1 MB.

## 2.2 Assembly and Precision

The three per-row scalars assemble into the weight norm:

$$w_{\text{norm}} = \sqrt{\max(\|\mathbf{W}\|_{\text{row}}^2 + 2s \cdot \text{cross} + s^2 \cdot \text{ba\_norm}, 0)} \quad (5)$$

The magnitude division is always computed in PyTorch after the kernel returns:

$$g \triangleq \mathbf{m} / \max(w_{\text{norm}}, \epsilon) \quad (6)$$

This ensures identical precision regardless of whether the Triton or PyTorch norm path produced  $w_{\text{norm}}$ , eliminating a source of fidelity divergence we observed at large activation scales (see §5.8).

All accumulation is performed in fp32 under `torch.no_grad()` with `autocast` disabled. Disabling `autocast` alone does not force fp32 when inputs are bf16, so each chunk of  $\mathbf{W}$ ,  $\mathbf{A}$ ,  $\mathbf{B}$ , and the intermediate  $\mathbf{U}_c$  is explicitly cast to fp32 before accumulation. This is consistent with the DoRA paper’s instruction (Section 4.3) to treat the norm as a detached constant [Liu et al., 2024]. We use  $g$  consistently throughout to denote the post-division scale, distinct from the learnable magnitude  $\mathbf{m}$ .

## 2.3 Complexity

Table 1 compares asymptotic and concrete memory costs.

**Why the measured reduction is smaller.** The dominant transient is the base-norm computation (Term 1 of Equation 2): the chunked  $\|\mathbf{W}\|_{\text{row}}^2$  accumulation creates a  $[d_{\text{out}}, \text{chunk\_size}]$  fp32 buffer that, at the default budget and  $d = 8192$ , approaches 256 MB, accounting for most of the 241 MB measured delta. This cost is *rank-independent*: identical at  $r = 16$  and  $r = 768$ . The theoretical reduction, which counts only rank-dependent tensors ( $\mathbf{U}$  and  $\mathbf{G}$ ), correctly predicts the asymptotic benefit as rank grows.

Since  $\mathbf{W}$  is frozen,  $\|\mathbf{W}\|_{\text{row}}^2$  could be precomputed into a  $[d_{\text{out}}]$  buffer (16 KB at  $d_{\text{out}} = 4096$ ), eliminating this transient entirely. We leave this caching for future work.

Table 1: The factored norm reduces rank-dependent persistent memory by  $15\times$  at  $d=8192$ ,  $r=512$  in fp32. Measured reductions are smaller ( $3.2\times$ ) because allocator deltas include the rank-independent base-norm transient (§2.3).

	PEFT	Factored (ours)
Rank-dependent persistent	$\mathcal{O}(d_{\text{in}}^2 + d_{\text{out}}d_{\text{in}})$	$\mathcal{O}(d_{\text{out}}r + r^2)$
Chunk buffer (transient)	Included above	$[d_{\text{out}}, \text{cs}]$ per chunk <sup>†</sup>
Per-module temps	3–4 dense $[d_{\text{out}}, d_{\text{in}}]$	$\mathbf{U}[d_{\text{out}}, r] + \mathbf{G}[r, r]$
Identity matrix	Every forward call	Never created
<i>Concrete: <math>d_{\text{out}} = d_{\text{in}} = 8192</math>, <math>r = 512</math>, fp32</i>		
Theory: dense (B@A)	256 MB	N/A
Theory: U + G	N/A	17.0 MB
<b>Theoretical reduction</b>		<b>15.1</b> $\times$
Measured: allocator delta	768 MB	241 MB
<b>Measured reduction</b>		<b>3.2</b> $\times$
<sup>†</sup> cs = $\min(d_{\text{in}}, \lfloor \text{budget} / (d_{\text{out}} \cdot 4) \rfloor)$ ; at 256 MB and $d=8192$ , cs spans full $d_{\text{in}}$ .		

**bf16 caveat.** The factored norm accumulates in fp32 regardless of weight dtype. Against half-precision PEFT baselines, this fp32 overhead inverts the isolated-norm memory ratio (PEFT/-factored) to  $0.8\times$  (i.e., factored uses *more* for the norm micro-operation in bf16). This does not negate model-level VRAM savings (Table 8), which include the fused compose kernel’s elimination of forward-pass intermediates.

**Compute tradeoff.** The factored norm is  $\sim 4.8\times$  slower than the dense reference when measured isolation (H200, fp32) because the reference performs a single contiguous `torch.linalg.norm` call, while the factored path uses multiple chunked matmuls. The system is faster end-to-end because the reference *first* materializes the full  $[d_{\text{out}}, d_{\text{in}}]$  product; it is this materialization, not the norm itself, that dominates time and memory. On lower-bandwidth hardware (RTX 6000 PRO, GDDR7), the factored norm matches or outperforms the reference at production ranks ( $r \leq 384$ ) for large weight matrices, so the  $4.8\times$  figure is a conservative bound.

### Algorithm 1: Factored Row-wise Norm

**Input:**  $\mathbf{W} \in \mathbb{R}^{d_{\text{out}} \times d_{\text{in}}}$  (frozen);  $\mathbf{A} \in \mathbb{R}^{r \times d_{\text{in}}}$ ,  $\mathbf{B} \in \mathbb{R}^{d_{\text{out}} \times r}$ ;  $s \in \mathbb{R}$ ;  $\varepsilon$  (dtype-dependent); `chunk_budget` (bytes, default 256 MB)

$cs \leftarrow \min(d_{\text{in}}, \lfloor \text{budget} / (d_{\text{out}} \cdot 4) \rfloor)$ , aligned to 64 elements.

All accumulation in fp32 under `torch.no_grad()`, autocast disabled. Cast  $\mathbf{W}$  chunks,  $\mathbf{A}$ ,  $\mathbf{B}$  to fp32 on the fly.

Initialize:  $\text{base\_sq} \leftarrow \mathbf{0}_{d_{\text{out}}}$ ,  $\text{cross} \leftarrow \mathbf{0}_{d_{\text{out}}}$ ,  $\mathbf{G} \leftarrow \mathbf{0}_{r \times r}$  (all fp32)

for each chunk  $c$  of size  $cs$ :

$\mathbf{W}_c = \mathbf{W}[:, c:c+cs].\text{float}()$   $[d_{\text{out}}, cs]$

$\mathbf{A}_c = \mathbf{A}[:, c:c+cs].\text{float}()$   $[r, cs]$

$\text{base\_sq} += (\mathbf{W}_c ** 2).\text{sum}(\text{dim}=1)$

$\mathbf{G} \leftarrow \mathbf{G} + \mathbf{A}_c \mathbf{A}_c^\top$

$\mathbf{U}_c \leftarrow \mathbf{W}_c \mathbf{A}_c^\top$   $[d_{\text{out}}, r]$  (not retained)

$\text{cross} += (\mathbf{B}.\text{float}() * \mathbf{U}_c).\text{sum}(\text{dim}=1)$

$\text{ba\_sq} = (\mathbf{B}.\text{float}() @ \mathbf{G} * \mathbf{B}.\text{float}()).\text{sum}(\text{dim}=1)$   $[d_{\text{out}}]$

$w_{\text{norm}} \leftarrow \sqrt{\max(\text{base\_sq} + 2s \cdot \text{cross} + s^2 \cdot \text{ba\_sq}, 0)}$   $[d_{\text{out}}]$

return  $w_{\text{norm}}.\text{to}(\text{input\_dtype})$

**Notes:** Chunk size aligns to 64 for Tensor Core MMA.  $\mathbf{U}_c$  is never stored for multiple chunks simultaneously. When  $s=0$ , `cross` and `ba_sq` are skipped;  $\mathbf{U}_c$  and  $\mathbf{G}$  are not allocated.  $\mathbf{G}$  is  $\leq 2.4$  MB at  $r = 768$  in fp32.

## 3 Fused Triton Kernels

### 3.1 Compose Kernel

The DoRA composition  $(g-1) \odot \text{base} + g \odot s \odot \text{lora}$  decomposes into four sequential element-wise operations in standard PyTorch, each launching a separate CUDA kernel: 3 reads + 1 write per op yields  $\sim 12$  memory passes total. The fused Triton [Tillet et al., 2019] kernel collapses these into a single pass: 3 reads (base, lora,  $g$ ) + 1 write, a  $\sim 4\times$  reduction in memory traffic. The realized speedup of 2.0–2.7 $\times$  (rather than 4 $\times$ ) reflects the fact that the eager path is partially latency-bound by kernel-launch gaps; the fused kernel achieves  $\sim 50\%$  of peak HBM bandwidth (Figure 7), vs.  $\sim 20\%$  for the eager path.

**Numerical stability.** The algebraically equivalent form  $g \odot (s \cdot \text{lora} + \text{base}) - \text{base}$  suffers from catastrophic cancellation when  $g \approx 1$ . This regime is not hypothetical. The stored magnitude parameters reflect the heterogeneous row norms of pretrained weights and naturally vary across layers and models, but DoRA initializes  $\mathbf{m} = \|\mathbf{W}\|_{\text{row}}$  and magnitudes track weight norms throughout training, so the composed scale  $g = \mathbf{m}/w_{\text{norm}}$  concentrates tightly around unity (mean  $\approx 1.0$ , std  $\approx 0.0015$ ). Measurement on a Qwen2-VL-7B adapter ( $r=128, 326$  modules, 1.77M elements) shows that 100% of  $g$  values fall in the bf16 collapse zone ( $|g-1| < \varepsilon_{\text{bf16}}/2$ ) and 20% in the fp16 zone: if  $(g-1) \odot \text{base}$  were evaluated in bf16, the base correction would vanish for every element; in fp16, for one in five.

The stable form  $(g-1) \odot \text{base} + g \odot s \odot \text{lora}$  keeps the small correction  $(g-1)$  explicit, but its precision advantage depends on fp32 intermediate computation to prevent  $(g-1)$  from rounding to zero. Both the Triton kernel and PyTorch fallback use this form with fp32 compute. Figure 1 shows 3.0 $\times$  lower peak error near  $g \approx 1$  compared to the naive alternative. Beyond the algebraic form,

## Numerical Stability: DoRA Compose at Near-Unity $g$ (shape 2048×8192, bf16)

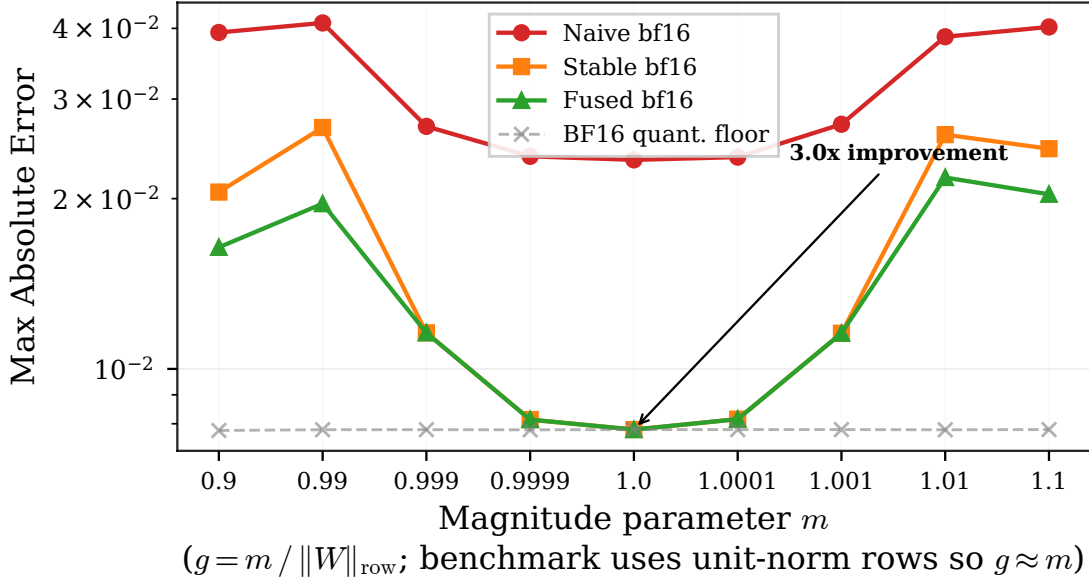


Figure 1: The stable compose form achieves  $3.0\times$  lower peak error near  $g \approx 1$  (bf16,  $d_{\text{out}} = 8192$ ,  $d_{\text{in}} = 2048$ ). The naive form  $g \odot (s \cdot \text{lora} + \text{base}) - \text{base}$  exhibits catastrophic cancellation; the stable form and fused kernel both remain near the bf16 quantization floor. Reference: fp64.

bf16 multiplication is non-associative: all code paths enforce a single canonical evaluation order ( $s \cdot \text{lora}$  first, then  $g \cdot (\cdot)$ ), ensuring bitwise parity across all PyTorch composition paths.

**Autotuning.** Optimal kernel configurations vary substantially across GPUs ( $\sim 9\%$  pairwise agreement across six GPUs), requiring per-device autotuning rather than a static table. First-run autotuning takes 10–30s per kernel, and caches persist in Triton’s default directory. Details in Appendix B.

### 3.2 Backward Kernel

The fused backward computes  $d_{\text{lora}} = g \cdot s \cdot d_{\text{out}}$  and  $d_{\text{base}} = (g-1) \cdot d_{\text{out}}$  in a single Triton pass. Two design decisions merit note:

- **Reduced ROWS\_PER\_PROGRAM:** Writing two output tensors doubles per-element traffic; reducing rows per program lowers register pressure and improves SM utilization.
- $d_{\text{mag}}$  via PyTorch reduction: The magnitude gradient uses a separate `.sum()` rather than `tl.atomic_add`, avoiding contention at large `num_rows` and the non-deterministic ordering of floating-point atomics.

### 3.3 Norm Assembly Kernel

A second Triton kernel fuses Equation 5, computing  $w_{\text{norm}}$  from the three factored terms. Store-reload barriers prevent FMA fusion, and an inline PTX `sqrt.rn.f32` instruction replaces Triton’s default approximate `sqrt`, exactly reproducing PyTorch’s evaluation order. The kernel stops at

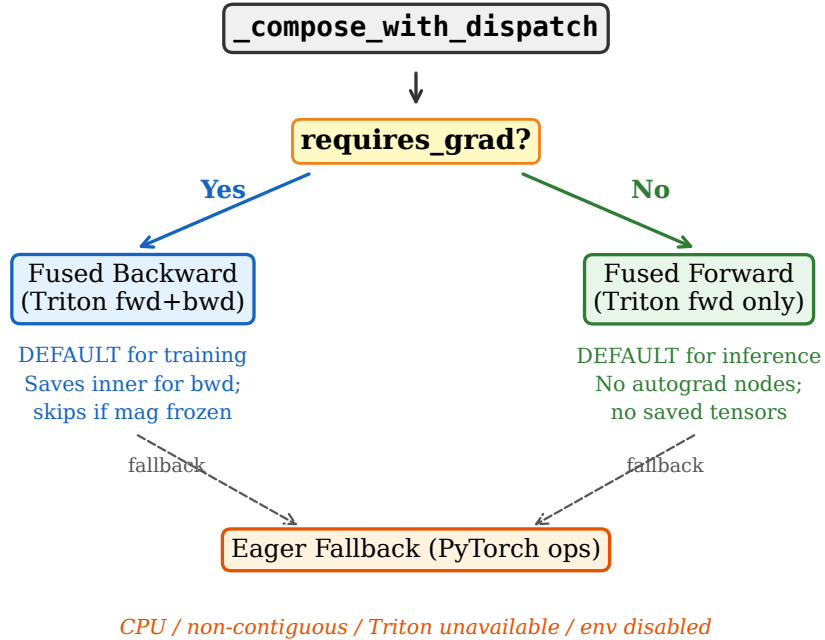


Figure 2: Three-tier dispatch: fused backward for training (Tier 1), fused forward for inference (Tier 2), eager fallback for CPU, no-Triton, or sub-crossover shapes (Tier 3).

Table 2: Dispatch tiers and their selection criteria.

Tier	Path	When	Tradeoff
1	Fused Backward	Training + CUDA + Triton + auto-gate/force-on	Fastest above crossover; saves <code>inner</code> for bwd
2	Fused Forward	Inference + CUDA + Triton	Speed without bwd memory
3	Eager Fallback	CPU / no Triton / force-off / sub-crossover	Universal compatibility

$w_{\text{norm}}$ ; the magnitude division (Equation 6) remains in PyTorch so both norm paths share the same precision context. Appendix C provides exact specifications for all three kernels.

## 4 Runtime Dispatch

The composition path is selected at runtime by `_compose_with_dispatch` (Figure 2, Table 2). Four environment variables control kernel availability and working-set budgets; defaults require no configuration.

**Tier 1 (Fused Backward).** A dual-output Triton kernel computes both the output and the saved tensor `inner = s·lora+base` in a single pass, eliminating the forward-pass VRAM spike from sequential PyTorch ops. When the magnitude is frozen (`requires_grad=False`), the `inner` allocation is skipped entirely. The default auto-mode crossover requires  $d_{\text{out}} \geq 2048$  and  $(\text{batch} \times \text{seq}) \times d_{\text{out}} \geq 2048 \times 6144$ ; smaller activations use Tier 3 because launch latency dominates. In the six evaluated

VLMs, KV projections ( $d_{\text{out}}$  as low as 512) fall below the crossover, so  $\sim 71\%$  of adapted modules per layer dispatch to Tier 1 during training and  $\sim 29\%$  fall back to Tier 3.

**Tier 2 (Fused Forward).** A forward-only Triton kernel with no autograd graph nodes, dispatched when `requires_grad` is false.

**Tier 3 (Eager Fallback).** Pure PyTorch; handles CPU, no-Triton, and sub-crossover training. Uses out-of-place composition when autograd is active to avoid aliasing.

**Precision.** All PyTorch compose paths produce bitwise-identical forward outputs by enforcing a single evaluation order. The Triton kernels preserve the same algebra but not bitwise equality (FMA contraction and reduction trees can perturb last bits); we treat Triton–PyTorch agreement as an empirical envelope: fp32 outputs stay within  $10^{-4}$  max-abs error, bf16/fp16 remain within dtype-appropriate tolerances (§5.8).

**Compatibility.** The fused compose is registered as a custom op (`peft::fused_dora_compose`) via `torch.library`, making the dispatch graph-break-free under `torch.compile` when dropout is inactive ( $p = 0$ ). DeepSpeed ZeRO-2/3 and FSDP1 are supported; FSDP2/DTensor is not (§6). The forward contract, `torch.compile` details, and the chunked-dropout path are specified in Appendices A and B.

**Magnitude division.** Across all tiers,  $g = \mathbf{m} / \max(w_{\text{norm}}, \epsilon)$  is computed in PyTorch outside the `no_grad` norm context, ensuring identical precision regardless of execution tier.

## 5 Experiments

### 5.1 Setup

Microbenchmarks use six GPUs spanning four architecture generations (Table 3); model-level benchmarks use three GPUs (RTX 6000 PRO, H200, B200) with sufficient VRAM for the tested models. All GPUs run identical software: PyTorch 2.10.0+cu130, Triton 3.6.0, Transformers 5.2.0, CUDA 13.1, driver 580.126.09. The PEFT baseline is upstream commit 20a9829 (v0.18.0.rc0).<sup>1</sup> Model-level benchmarks exclude the optimizer step to isolate DoRA overhead and use a partial-sequence loss (1024 loss tokens) to match production RLHF/GRPO memory profiles; full-sequence loss creates a 6–12 GB logit spike that masks adapter working-set differences. A sensitivity check at 4096 loss tokens confirms speedups are unchanged. Each microbenchmark reports the median of 200 CUDA-event-timed trials (10 warmup); model-level benchmarks use 20 repeats (3 warmup, CV < 1.7%). Memory measurement methodology and full reproducibility instructions are provided in Appendix D.

### 5.2 Model-Level Performance

Table 4 summarizes the headline result: gradient-computation speedup across six 8–32B VLMs on three GPUs. The fused implementation is 1.46–1.87 $\times$  faster than HF PEFT’s DoRA implementation and 1.18–1.24 $\times$  faster than our own eager baseline, with 1.3–6.7 GB lower peak VRAM (Table 8). These timings cover forward+backward only (excluding optimizer updates), so the end-to-end

---

<sup>1</sup>Later HEAD 9cf86c7 (2026-02-24) is algorithmically identical for training; see §7.

Table 3: Benchmark hardware. “Micro”: microbenchmark coverage. “Model”: full model-level gradient-computation and inference benchmarks.

GPU	Arch	Memory	BW (TB/s)	Scope
L40S	SM89 Ada	48 GB GDDR6	0.86	Micro
A100-SXM4	SM80 Ampere	80 GB HBM2e	2.04	Micro
RTX 6000 PRO	SM120 Blackwell	96 GB GDDR7	1.60	Micro+Model
H200	SM90 Hopper	141 GB HBM3e	4.80	Micro+Model
B200	SM100 Blackwell	192 GB HBM3e	7.70	Micro+Model
B300	SM103 Blackwell	268 GB HBM3e	7.70	Micro

Table 4: Gradient-computation speedup on 8–32B VLMs ( $r = 384$ ,  $\text{bf16}$ ,  $\text{seq}=4096$ ,  $\text{bs}=1$ ,  $\text{ga}=8$ ,  $\text{loss\_tokens}=1024$ , 20 repeats). The HF PEFT DoRA baseline takes 46–87% longer per iteration than fused. 32B models OOM on RTX 6000 PRO (96 GB) under all configurations. See Table 5 for absolute times.

Model	Speedup vs. PEFT DoRA			Speedup vs. Eager		
	RTX	H200	B200	RTX	H200	B200
Qwen2.5-VL-32B	OOM	1.73×	1.74×	OOM	1.20×	1.22×
Qwen3-VL-32B	OOM	1.66×	1.67×	OOM	1.18×	1.21×
Qwen3.5-27B	1.51×	1.57×	1.57×	1.22×	1.21×	1.23×
Gemma3-27B	1.53×	1.61×	1.56×	1.20×	1.19×	1.21×
Mistral-Sm-24B	1.66×	1.87×	1.87×	1.22×	1.21×	1.23×
Qwen3-VL-8B	1.46×	1.50×	1.47×	1.23×	1.21×	1.24×

Table 5: Absolute gradient-computation time (seconds). Each iteration covers 8 gradient-accumulation micro-steps; 32 768 tokens total. Standard deviations  $\leq 0.13$  s (CV < 1.7%).

Model	Fused (s)			Eager (s)			PEFT (s)		
	RTX	H200	B200	RTX	H200	B200	RTX	H200	B200
Qwen2.5-VL-32B	OOM	30.9	23.3	OOM	37.1	28.5	OOM	53.6	40.4
Qwen3-VL-32B	OOM	33.4	25.4	OOM	39.5	30.6	OOM	55.4	42.3
Qwen3.5-27B	39.5	25.4	19.4	48.1	30.6	23.9	59.5	39.8	30.5
Gemma3-27B	41.6	27.5	21.4	50.0	32.7	25.8	63.6	44.1	33.4
Mistral-Sm-24B	32.5	20.9	15.9	39.7	25.2	19.6	53.9	39.1	29.8
Qwen3-VL-8B	12.9	9.1	7.1	15.9	11.0	8.8	18.8	13.7	10.5

wall-clock gain is smaller: in the 2000-step convergence run, the same optimization reduced total training time by 8.3% once optimizer, data loading, and framework overhead were included (§5.9). The 32B models exceed the 96 GB RTX 6000 PRO under *all* configurations; this is a capacity limit, not a method-specific regression.

**Inference.** Inference speedup is higher than gradient computation: 1.5–2.0× over PEFT, 1.14–1.20× over eager (Figure 4), because the forward pass concentrates the compose savings without dilution from backward-pass work. RTX 6000 PRO runs inference on all six models including 32B (84–88 GB peak), which OOM during gradient computation.

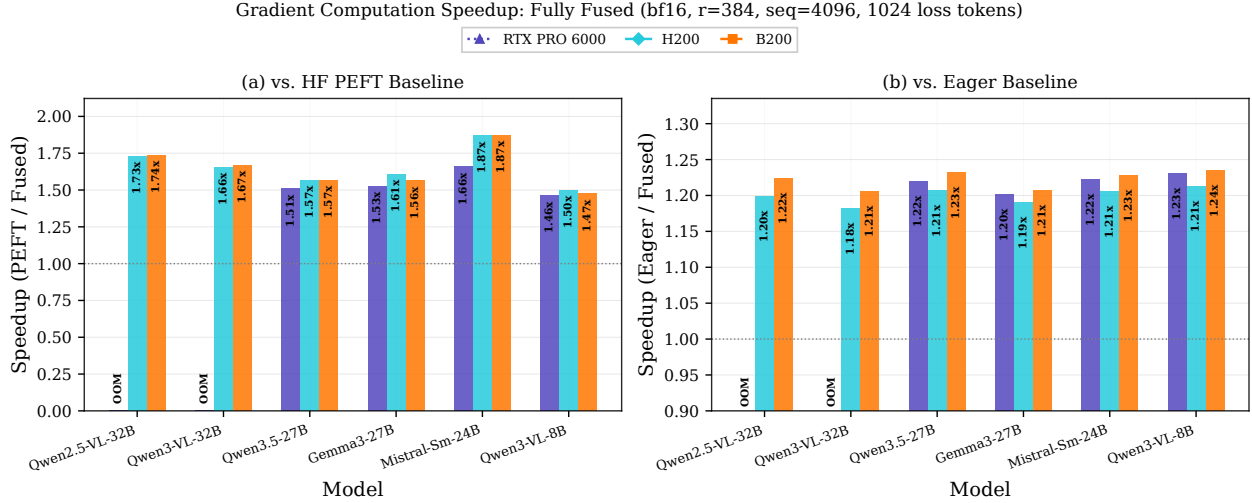


Figure 3: Gradient-computation speedup across six VLMs on three GPUs (bf16,  $r=384$ , seq=4096). (a) Fused vs. the HF PEFT DoRA baseline: 1.46–1.87 $\times$ . (b) Fused vs. eager: 1.18–1.24 $\times$ . 32B models OOM on RTX 6000 PRO under all configurations.

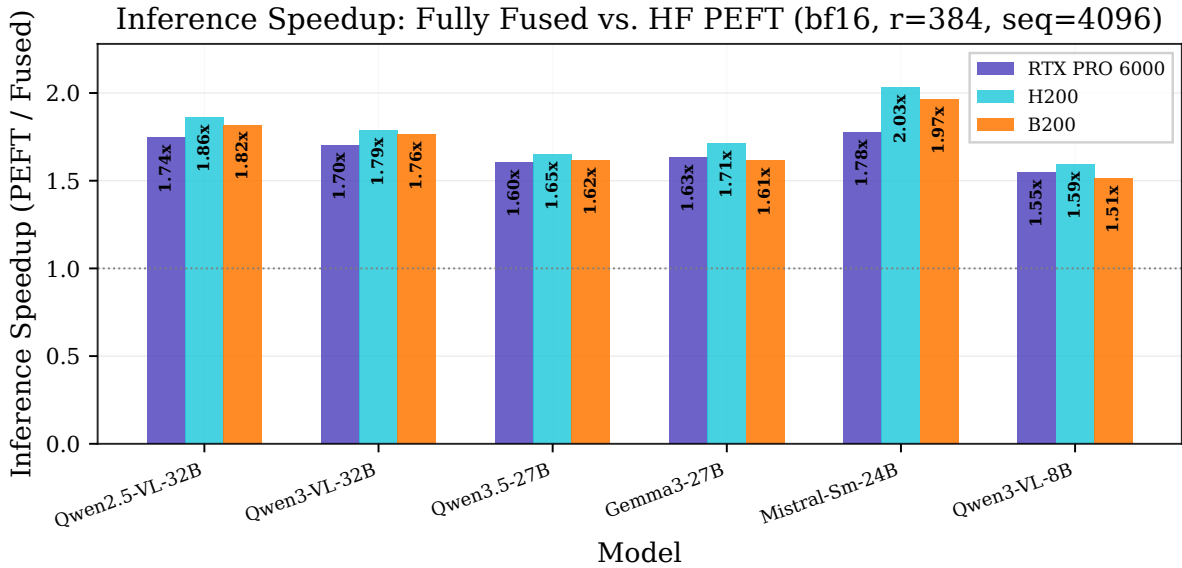


Figure 4: Inference speedup: 1.5–2.0 $\times$  over the HF PEFT DoRA baseline. All six models run on all three GPUs, including 32B on RTX 6000 PRO (96 GB) that OOM during gradient computation.

**High-rank scaling.** Table 6 validates the high-rank framing at  $r=384$ , 512, and 768. Speedup vs. PEFT DoRA *increases* with rank for the 32B model (1.66 $\times$   $\rightarrow$  1.74 $\times$ ) because PEFT’s materialization cost grows with  $r$ , while the factored norm’s rank-dependent overhead ( $\mathbf{U}$  and  $\mathbf{G}$ ) remains small. Speedup vs. eager decreases modestly (1.18 $\times$   $\rightarrow$  1.14 $\times$ ) as larger LoRA matmuls dilute the compose kernel’s contribution.

Table 6: Speedup vs. the HF PEFT DoRA baseline grows with rank; speedup vs. eager decreases modestly (H200, bf16, seq=4096, 20 repeats).

Model	Rank	vs. PEFT DoRA		vs. Eager	
		Grad.	Infer.	Grad.	Infer.
Qwen3.5-27B	384	1.57×	1.65×	1.21×	1.16×
	512	1.61×	1.68×	1.18×	1.14×
	768	1.53×	1.59×	1.15×	1.11×
Qwen3-VL-32B	384	1.66×	1.78×	1.18×	1.14×
	512	1.70×	1.82×	1.16×	1.12×
	768	1.74×	1.87×	1.14×	1.10×

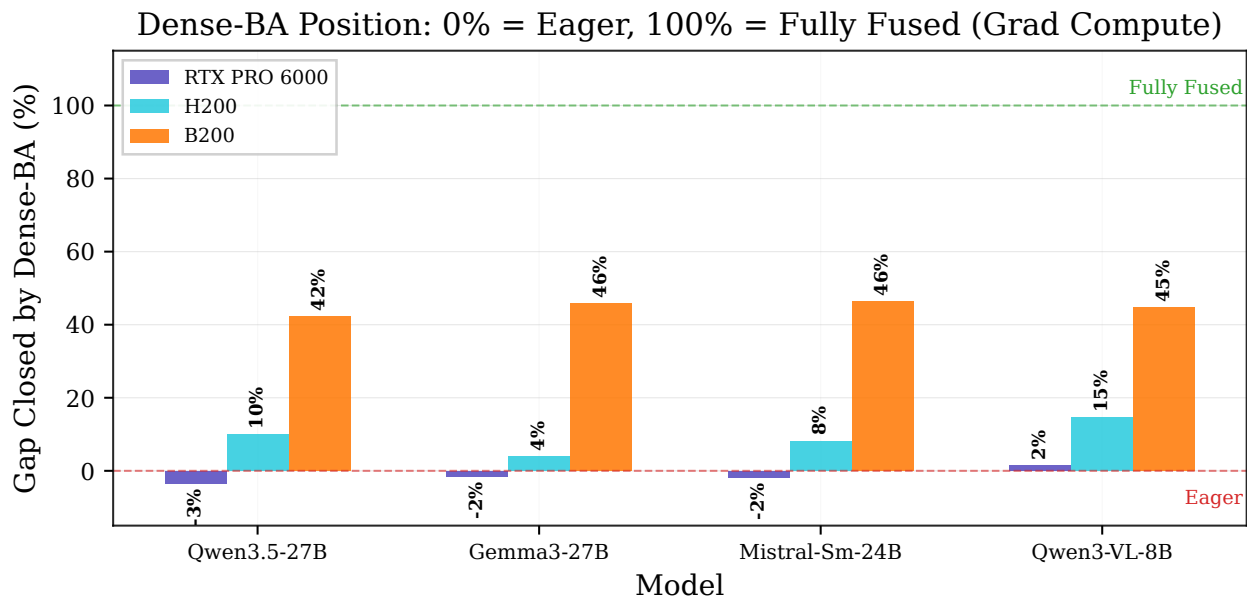


Figure 5: Dense (B@A) position in the eager-to-fused gap (0% = eager, 100% = fused). Negative values: dense (B@A) is *slower* than eager. The benefit is GPU-bandwidth-sensitive; the factored approach is robust.

### 5.3 Why Dense (B@A) Is Not Enough

Computing `lora_B.weight @ lora_A.weight` directly (the most obvious fix) eliminates the identity matrix but still materializes the full  $[d_{\text{out}}, d_{\text{in}}]$  product. Figure 5 shows that dense (B@A) captures 0% of the eager-to-fused gap on some model/GPU combinations and is sometimes *slower* than the eager baseline. Dense (B@A) also uses 1–2 GB more peak VRAM than fused on all tested models. The full factored norm is necessary for consistent gains across GPU architectures.

### 5.4 Compose Kernel Performance

Figure 6 shows compose speedup across activation sizes on six GPUs. Geometric mean forward speedup (bf16, all 20 shapes):  $2.70\times$  B200,  $2.62\times$  B300,  $2.00\times$  H200,  $1.92\times$  RTX 6000 PRO,  $1.73\times$  A100,  $1.47\times$  L40S. The consistency from GDDR6 (0.86 TB/s) to HBM3e (7.7 TB/s) confirms the gains derive from reduced memory traffic rather than architecture-specific effects.

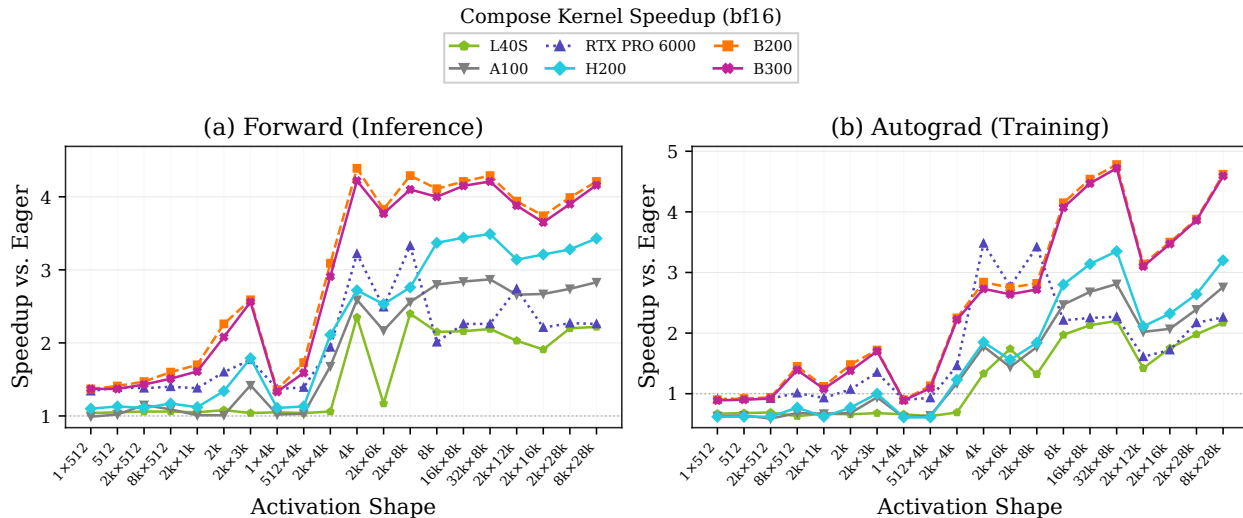


Figure 6: Compose kernel speedup vs. eager (bf16) across six GPUs. (a) Forward: 1.5–4.5 $\times$ . (b) Autograd: gains compound with activation size.

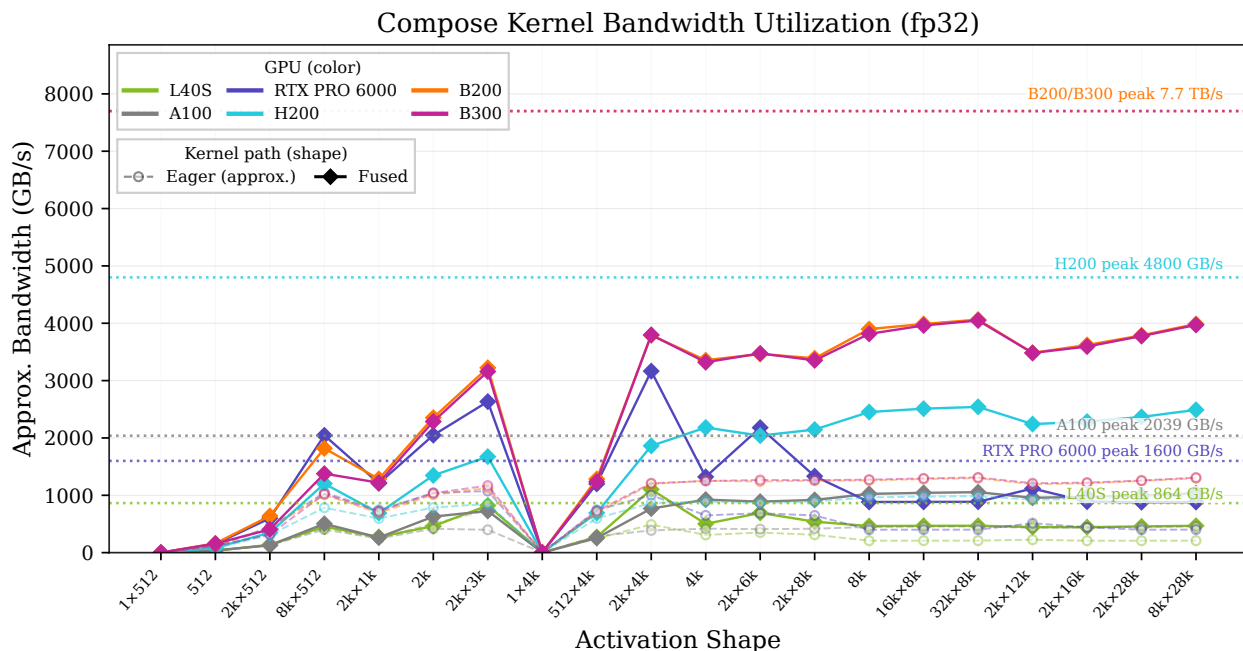


Figure 7: Bandwidth utilization (fp32, six GPUs). Fused approaches  $\sim$ 50% of peak on all architectures; eager values are approximate lower bounds.

**Bandwidth utilization.** The fused kernel achieves 3950–4070 GB/s on B200/B300 ( $\sim$ 53% of peak), 2490–2540 GB/s on H200 ( $\sim$ 53%), 1040–1050 GB/s on A100 ( $\sim$ 52%), 880–890 GB/s on RTX 6000 PRO ( $\sim$ 55%), and 460–470 GB/s on L40S ( $\sim$ 54%) at the largest shapes (Figure 7). On B200, the eager path reaches only 17% of peak, yielding the largest absolute bandwidth gap. Throughput scales nearly linearly with peak bandwidth across the full 0.86–7.7 TB/s range, confirming these kernels are memory-bandwidth-bound.

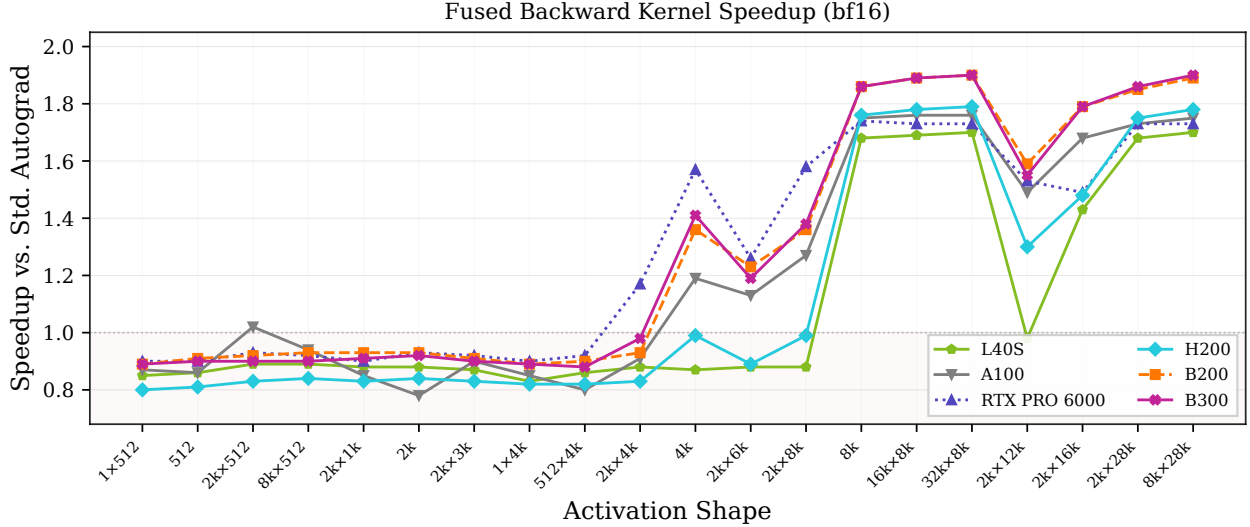


Figure 8: Backward speedup (bf16). Below  $\sim 4096 \times 4096$ , launch overhead dominates; above  $\sim 8192 \times 8192$ , fused wins on all GPUs.

Table 7: Norm memory: measured allocation delta and theoretical reduction (fp32, H200). Measured reductions are smaller than theoretical because they include the rank-independent base-norm transient (§2.3).

Shape	Rank	PEFT	Factored	Meas. $\times$	Theory $\times$
$4096 \times 4096$	64	192 MB	65 MB	3.0 $\times$	63 $\times$
$4096 \times 4096$	384	192 MB	71 MB	2.7 $\times$	9.8 $\times$
$4096 \times 4096$	512	192 MB	73 MB	2.6 $\times$	7.1 $\times$
$8192 \times 8192$	384	768 MB	245 MB	3.1 $\times$	20.4 $\times$
$8192 \times 8192$	512	768 MB	241 MB	3.2 $\times$	15.1 $\times$
$8192 \times 8192$	768	768 MB	236 MB	3.2 $\times$	9.8 $\times$
$4096 \times 11008$	384	516 MB	179 MB	2.9 $\times$	26.2 $\times$
$8192 \times 28672$	384	2688 MB	245 MB	11.0 $\times$	71.3 $\times$

## 5.5 Backward Kernel Performance

The backward kernel shows a clear crossover: below  $\sim 2048 \times 6144$  (rows  $\times d_{\text{out}}$ ), launch overhead dominates and fused can trail eager (0.88–0.99 $\times$ ); above  $\sim 8192 \times 8192$ , fused wins on all six GPUs (Figure 8). Geometric mean speedup (bf16, all shapes): 1.23 $\times$  B200, 1.22 $\times$  B300/RTX 6000 PRO, 1.16 $\times$  A100, 1.08 $\times$  H200, 1.06 $\times$  L40S. Gradient correctness: fp32  $d_{\text{lor}}$  and  $d_{\text{base}}$  match the eager baseline at tolerance floor;  $d_{\text{mag}}$  shows  $\leq 2.14 \times 10^{-4}$  difference due to the separate reduction path.

## 5.6 Norm Memory Reduction

Figure 9 and Table 7 show both theoretical and measured memory reductions. The  $8192 \times 28672$  MoE shape achieves 11 $\times$  measured reduction. The factored norm’s latency tradeoff (Figure 10) is hardware-dependent: on RTX 6000 PRO, factored matches or outperforms the reference at  $r \leq 384$  for  $8192 \times 8192$  matrices.

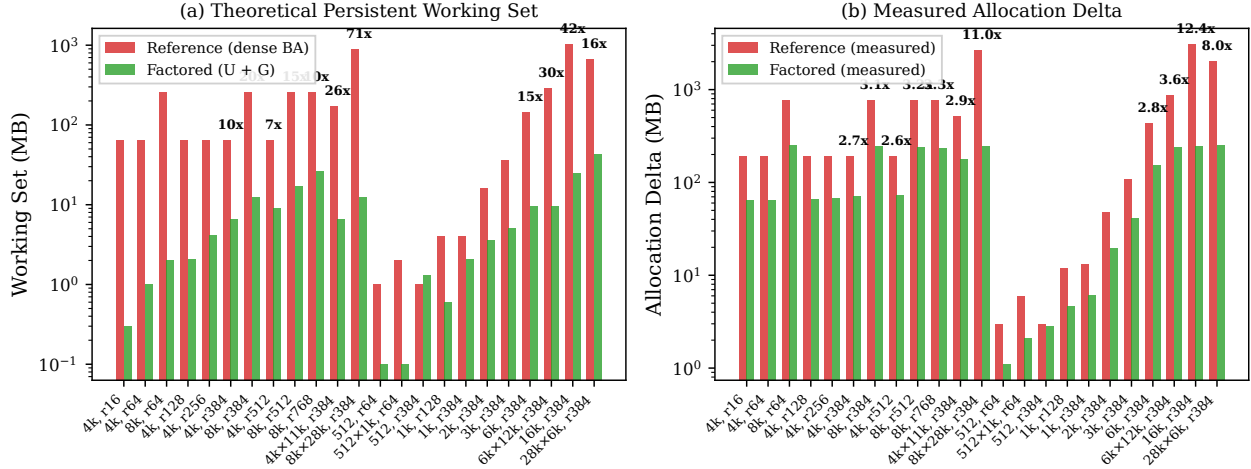


Figure 9: Norm memory reduction. (a) Theoretical persistent working set. (b) Measured allocator delta. The MoE shape  $8192 \times 28672$  achieves 11 $\times$  measured reduction.

RTX PRO 6000: Norm Computation Latency vs. Rank

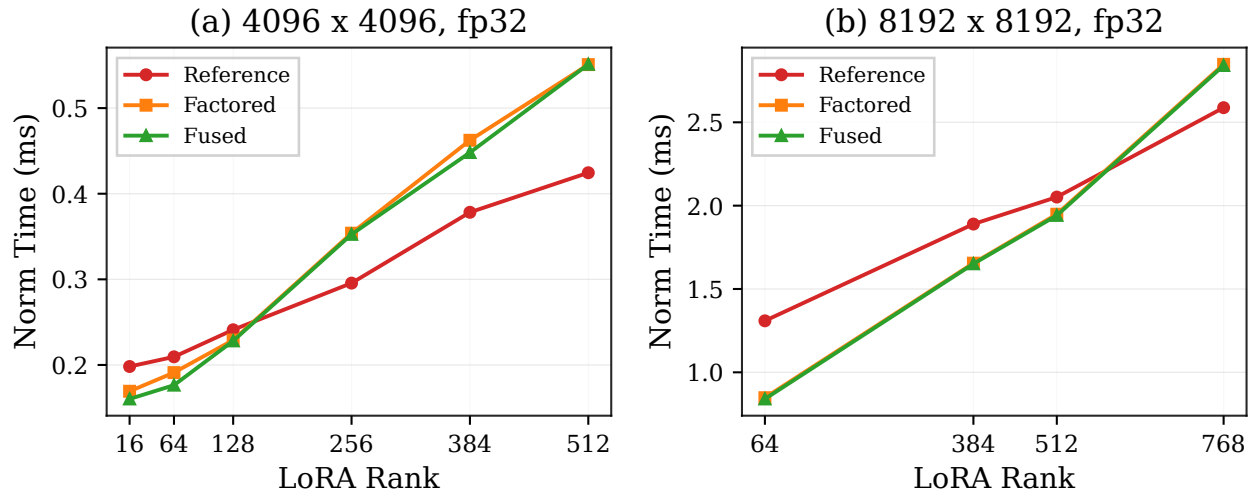


Figure 10: Norm latency vs. rank (RTX 6000 PRO, fp32). The PEFT time is constant in  $r$ ; factored scales linearly. At  $r \leq 128$ , factored matches the reference due to reduced memory traffic.

## 5.7 Memory Profile

The fused backward path reduces forward peak VRAM by eliminating intermediate materialization while maintaining identical backward peak (Figure 11). At the model level (Table 8), fused uses 0.1–1.0 GB less peak VRAM than eager and 1.2–6.7 GB less than PEFT. Dense (B@A) uses more peak VRAM than fused on all models.

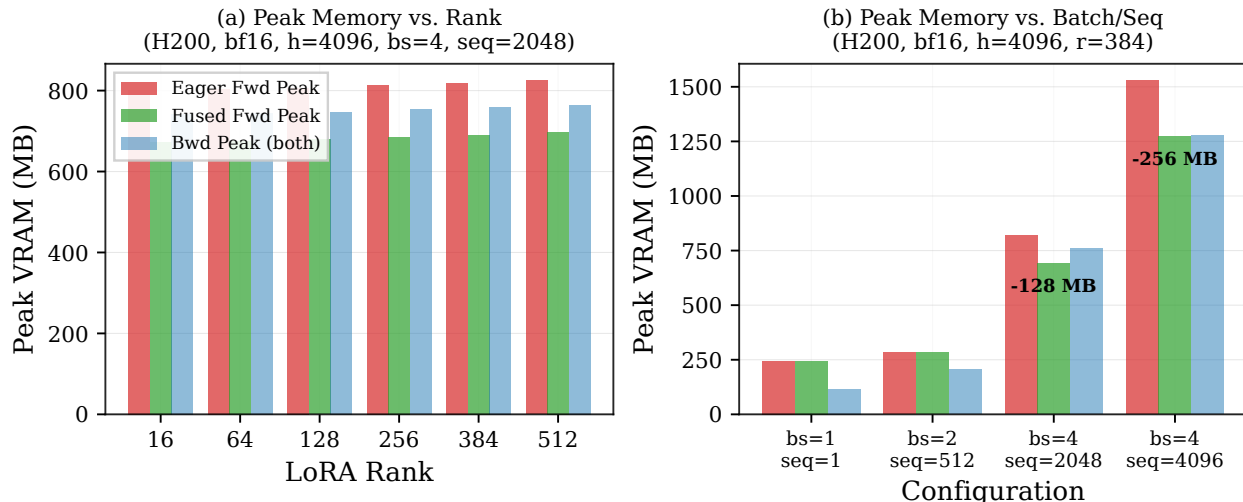


Figure 11: Memory profile (H200, bf16,  $d=4096$ ,  $bs=4$ ,  $seq=2048$ ). (a) Fused reduces forward peak by 64 MB. (b) Savings grow with batch $\times$ seq; backward peak is unchanged.

Table 8: Model-level peak VRAM (GB). Fused uses less than all baselines on every model. 32B models OOM on RTX 6000 PRO.

Model	Method	RTX	H200	B200
Qwen2.5-VL-32B	Eager	OOM	99.2	99.2
	Fused	OOM	98.4	98.4
	Dense (B@A)	OOM	100.6	100.6
	PEFT	OOM	103.5	103.5
Mistral-Sm-24B	Eager	71.6	71.7	71.6
	Fused	70.6	70.7	70.6
	Dense (B@A)	73.3	73.4	73.3
	PEFT	77.3	77.4	77.3
Qwen3-VL-8B	Eager	29.8	29.9	29.8
	Fused	29.5	29.5	29.5
	Dense (B@A)	30.1	30.2	30.1
	PEFT	30.7	30.8	30.7

Full table (all 6 models) in Appendix E.

## 5.8 Cross-Architecture Consistency

Table 9 summarizes microbenchmark speedups across all six GPUs. Model-level eager/fused speedups range from  $1.18\times$  to  $1.24\times$  with cross-GPU CV  $< 2\%$ , providing stronger statistical evidence than additional repeats on a single GPU.

**Fidelity.** Cosine similarity between fused and eager final logits exceeds 0.9999 for all six models on all three GPUs ( $\cos \geq 0.999996$  on HBM-class GPUs). An earlier code version showed reduced fidelity on Gemma-3-12B ( $\cos = 0.991\text{--}0.999$ ); the root cause was fusing the magnitude division into Triton, which allowed FMA contraction and approximate `sqrt` to perturb rounding at large

Table 9: Geometric mean microbenchmark speedups (all shapes, 200 repeats). Norm memory  $0.8\times$  in bf16 means factored uses *more* memory for the isolated norm due to fp32 accumulation transients (§2.3).

	Compose fwd	Backward	E2E	Norm mem
L40S bf16	$1.47\times$	$1.06\times$	$1.05\times$	$0.8\times$
A100 bf16	$1.73\times$	$1.16\times$	$1.07\times$	$0.8\times$
RTX 6000 PRO bf16	$1.92\times$	$1.22\times$	$1.08\times$	$0.8\times$
H200 bf16	$2.00\times$	$1.08\times$	$1.06\times$	$0.8\times$
B200 bf16	$2.70\times$	$1.23\times$	$1.08\times$	$0.8\times$
B300 bf16	$2.62\times$	$1.22\times$	$1.08\times$	$0.8\times$

fp32 rows in Appendix F.

Table 10: Multi-seed convergence: eager vs. fused training loss (Qwen3.5-9B-Base,  $r = 384$ , 2000 steps). Grand mean per-step delta  $7.1 \times 10^{-4}$ ; final eval losses agree to  $< 1.5 \times 10^{-4}$ .

Seed	Steps	Mean $ \Delta $	Max $ \Delta $	Eval $ \Delta $	Wall (fused/eager)
1	2000	$7.2 \times 10^{-4}$	$1.1 \times 10^{-2}$	$9.2 \times 10^{-5}$	330/362 min
2	2000	$6.9 \times 10^{-4}$	$3.3 \times 10^{-3}$	$1.4 \times 10^{-4}$	330/359 min
3	2000	$7.1 \times 10^{-4}$	$4.1 \times 10^{-3}$	$3.3 \times 10^{-5}$	330/359 min
<i>Grand mean</i>		$7.1 \times 10^{-4}$	—	$8.9 \times 10^{-5}$	330/360 min

activation scales. De-fusing the division (§4), adding store-reload barriers, and replacing the `sqrt` with inline PTX resolved the discrepancy, improving fidelity to  $\cos > 0.9999$  across all GPUs.

## 5.9 Convergence Equivalence

To verify that fused kernels do not affect training dynamics, we trained controlled SFT experiments on a length-filtered derivative of MMFineReason-SFT-123K [Lin et al., 2026] using Qwen3.5-9B-Base, DoRA  $r = 384$ ,  $\alpha = 192$ , rsLoRA, bf16, AdamW, ZeRO-2, gradient checkpointing,  $bs = 3$ ,  $ga = 2$ ,  $seq = 5120$ , 2000 steps on a single RTX 6000 PRO, using the SWIFT framework [Zhao et al., 2024], with three seeds ( $\times$  eager/fused = 6 runs). Table 10 and Figure 12 summarize the results.

The worst-case single-step delta ( $1.1 \times 10^{-2}$ , seed 1, step 398) is a transient early-training divergence that does not propagate: by step 1000, all deltas fall below  $3.3 \times 10^{-3}$ . Gradient norms track identically, confirming that the  $d_{mag}$  reduction-ordering difference does not accumulate over 2000 steps.

**Wall-clock.** The fused path completed 2000 steps in 330 min compared with 360 min for the eager baseline (8.3% reduction), consistent with the 21% gradient-computation speedup diluted by optimizer steps, data loading, and framework overhead.

**Cross-model and cross-optimizer check.** An additional pair on Qwen3-VL-8B-Instruct with Muon+AdamW ( $r = 256$ , single seed) showed consistent results: mean  $|\Delta_{loss}| = 7.7 \times 10^{-4}$ , final eval  $|\Delta| = 3.9 \times 10^{-5}$ , 8.2% wall-clock reduction.

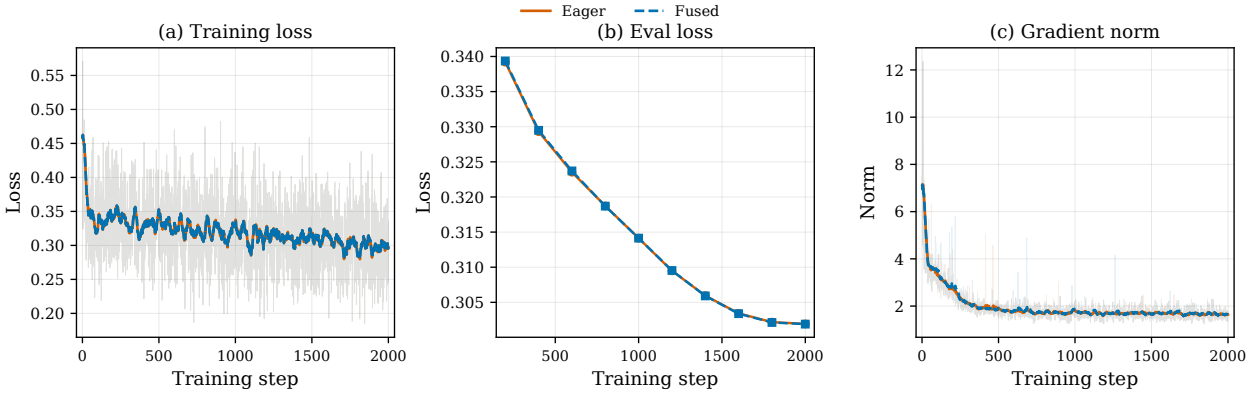


Figure 12: Convergence: eager vs. fused are visually indistinguishable (Qwen3.5-9B-Base,  $r=384$ , seed 3 of 3). (a) Training loss (25-step smoothing). (b) Eval loss (200-step intervals). (c) Gradient norms.

## 6 Discussion

### 6.1 Deployment Context

The factored norm is particularly valuable when training and inference compete for GPU memory. Our GRPO [Shao et al., 2024] pipeline co-locates vLLM [Kwon et al., 2023] (tensor-parallel inference) alongside DoRA fine-tuning ( $r=384$ ) of a 38B VLM on  $4\times B200$  (192 GB each), with large global batches under ZeRO-2 and gradient checkpointing. After vLLM reserves its KV-cache allocation, training headroom per GPU is tight; the memory challenge is cumulative rather than catastrophic. Each of the 500+ adapted modules re-materializes its norm temporaries during gradient checkpointing recomputation, and the resulting transient allocations fragment the caching allocator. Cross-device bandwidth, already under pressure from gradient all-reduce and tensor-parallel inference communication, leaves little margin for the additional memory traffic of dense per-module materialization. The factored norm eliminates these transients, and we observed no numerical drift attributable to fusion. (This is an illustrative anecdote and was not benchmarked under the methodology of §5.)

### 6.2 Tradeoffs and Limitations

Table 11 consolidates practitioner recommendations.

**Where fusion offers no advantage.** Below  $\sim 2048 \times 6144$  activations, launch latency dominates; the dispatch encodes this crossover conservatively. On non-CUDA platforms, Triton kernels are unavailable.

**Fused backward VRAM.** The fused backward saves one activation-sized tensor (*inner*) per module, but the dual-output kernel also eliminates the forward-pass spike from sequential ops. Net effect: fused uses 0.1–1.0 GB *less* peak VRAM than eager at the model level. With frozen magnitude, *inner* is spilled entirely.

**Numerical precision.** All PyTorch compose paths are bitwise identical. Triton preserves the same algebra but not bitwise equality (§4). Residual drift concentrates in  $d_{\text{mag}}$  reductions rather

Table 11: Recommended configuration by scenario.

Scenario	Config	Rationale
Training, CUDA, above crossover	Tier 1 (fused bwd)	Full speedup; 0.1–1.0 GB <i>less</i> VRAM than eager
Training, memory-constrained	Tier 1 + frozen mag	<b>inner</b> skipped; lower peak VRAM
Inference, CUDA	Tier 2 (fused fwd)	Compose speedup, no backward memory
CPU / no Triton	Tier 3 (eager)	Automatic fallback
$r \geq 384$ , any single GPU	Factored norm	PEFT path 46–87% slower
$r \leq 64$ , $d \leq 4096$	Either norm	Factored overhead minimal
Colocated train + infer	Factored norm	Dense temporaries compete with inference budget

than pointwise compose. Convergence studies (§5.9) confirm these differences do not accumulate.

**Distributed training.** DeepSpeed ZeRO-2/3 and FSDP1 are supported. FSDP2/DTensor is not: the factored norm assumes access to the full base weight  $\mathbf{W}$ . Extending to FSDP2 would require distributed accumulation of the chunk-wise partial sums followed by an all-reduce over the shard dimension; the per-row output ( $[d_{\text{out}}]$ ) is small enough to replicate. We leave this for future work.

**Embedding formula correction.** PEFT’s embedding path computes only  $g \odot \text{lora} \cdot s$ , omitting  $(g-1) \odot \text{base}$ . Our implementation applies the full DoRA formula consistently across all layer types. No headline benchmarks include adapted embeddings; checkpoints fine-tuned with PEFT’s embedding path may require re-fine-tuning or a legacy composition fallback.

**Ablation.** Model-level speedups reflect both contributions (factored norm + fused kernels) jointly. Microbenchmarks (Tables 9 and 7) provide component-level measurements, and the model-level eager-vs.-fused comparison provides a partial ablation of the kernel-fusion contribution. A fuller factorial ablation across additional model families would strengthen the evidence.

## 7 Related Work

**Parameter-efficient fine-tuning.** LoRA [Hu et al., 2022] introduced low-rank adapter decomposition; DoRA [Liu et al., 2024] adds magnitude-direction separation. rsLoRA [Kalajdziewski, 2023] provides rank-stabilized scaling that interacts with our factored norm ( $s$  appears in all three terms of Equation 2).

**DoRA variants.** EDoRA [Nasiri and Garraghan, 2025] reduces static parameter count via SVD; DoRAN [Diep et al., 2025] injects noise into the normalization denominator. Both address statistical efficiency rather than transient memory; our optimization is complementary. Chronicals [Nair, 2026] and LoRAFusion [Zhu et al., 2026] fuse LoRA-related operations but do not target the DoRA-specific norm or composition.

**Framework implementations.** Every major framework we checked (HF PEFT, torchtune, Unsloth, SWIFT, LLaMA-Factory, Axolotl) uses the same `torch.eye` materialization pattern. Unsloth explicitly disables its custom kernels when DoRA is active; orchestration frameworks delegate entirely to PEFT. As of February 2026, no existing framework avoids materializing the dense **BA** product (Appendix G).

**Kernel fusion.** FlashAttention [Dao et al., 2022, Dao, 2024] demonstrated that tiled, fused kernels improve both speed and memory for attention. Liger Kernel [Hsu et al., 2024] applies similar principles to cross-entropy, SwiGLU, and RMSNorm. Our work targets the DoRA composition, a simpler (element-wise with broadcasting) but equally memory-bound pattern. The algebraic identity underlying the factored norm (expanding a sum-of-squares into base, cross, and Gram terms) is standard in numerical linear algebra; our contribution is its application to the DoRA-specific computation with dtype discipline, chunking, and integration into the fused pipeline.

**LLM-guided optimization.** Meta’s KernelAgent [PyTorch, 2025] confirmed our compose kernel is near-roofline (89% memory bandwidth SOL, 1.5% improvement). For the backward, KernelAgent discovered a two-stage partial-reduction strategy that fuses the  $d_{\text{mag}}$  reduction, achieving  $3.58\times$  over eager (88.5% SOL) vs. our  $1.06\text{--}1.23\times$ . Our release prioritizes drop-in compatibility and end-to-end wins across real models; integrating that pattern is a direct avenue for future work. KernelAgent’s generated listings are included in `code/kernelagent_sols`.

## 8 Conclusion

We presented a systems implementation of DoRA: a factored norm that reduces working memory from  $\mathcal{O}(d_{\text{out}} \times d_{\text{in}})$  to  $\mathcal{O}(d_{\text{out}} \times r + r^2)$ , and fused Triton kernels that collapse multi-step composition into single-pass GPU operations.

On six 8–32B VLMs, the fused implementation is  $1.5\text{--}2.0\times$  faster than HF PEFT’s DoRA implementation for inference, and  $1.5\text{--}1.9\times$  faster for gradient computation (optimizer step excluded), with up to 7 GB lower peak VRAM. Microbenchmarks on six GPUs spanning four architecture generations confirm  $1.5\text{--}2.7\times$  compose-kernel speedup. Fidelity holds at three levels: operator tests within quantization-aware bounds, final-logit  $\cos > 0.9999$ , and matched training curves across seeds.

**Known limitations.** FSDP2 is unsupported. Convergence validation covers two model families, two optimizers, and one dataset in the SFT regime; generalization to RL pipelines remains to be confirmed. Model-level benchmarks cover three of six GPUs; L40S, A100, and B300 have microbenchmark coverage only. The dispatch crossover is an empirical heuristic that may need retuning for future hardware.

## Data Availability

All source code, benchmark scripts, raw JSON results, Triton autotune caches, and figure generation scripts are available at <https://github.com/socketeye44/dorafactors> (tag v1.0). The convergence validation uses a public dataset (MMFineReason-SFT-123K; Lin et al. 2026) for fully reproducible confirmation. The authors declare no competing interests.

## Acknowledgements

This work was developed through extensive collaborative programming with Claude Opus 4.6 (Anthropic), which contributed to kernel implementation, test design, numerical analysis, and iterative debugging. The authors take full responsibility for the accuracy and integrity of the work.

## References

- Jason Ansel, Edward Yang, Horace He, Natalia Gimelshein, Animesh Jain, Michael Voznesensky, Bin Bao, Peter Bell, David Berard, Evgeni Burovski, et al. PyTorch 2: Faster machine learning through dynamic Python bytecode transformation and graph compilation. In *Proceedings of the 29th ACM International Conference on Architectural Support for Programming Languages and Operating Systems*, volume 2 of *ASPLOS '24*. ACM, 2024. doi: 10.1145/3620665.3640366.
- Tianqi Chen, Bing Xu, Chiyuan Zhang, and Carlos Guestrin. Training deep nets with sublinear memory cost. *arXiv preprint arXiv:1604.06174*, 2016.
- Tri Dao. FlashAttention-2: Faster attention with better parallelism and work partitioning. In *International Conference on Learning Representations*, 2024. arXiv:2307.08691.
- Tri Dao, Daniel Y. Fu, Stefano Ermon, Atri Rudra, and Christopher Ré. FlashAttention: Fast and memory-efficient exact attention with IO-awareness. In *Advances in Neural Information Processing Systems*, volume 35, pages 16344–16359, 2022. arXiv:2205.14135.
- Nghiem T. Diep, Hien Dang, Tuan Truong, Tan Dinh, Huy Nguyen, and Nhat Ho. DoRAN: Stabilizing weight-decomposed low-rank adaptation via noise injection and auxiliary networks. *arXiv preprint arXiv:2510.04331*, 2025.
- Pin-Lun Hsu, Yun Dai, Vignesh Kothapalli, Qingquan Song, Shao Tang, Siyu Zhu, Steven Shimizu, Shivam Sahni, Haowen Ning, and Yanning Chen. Liger kernel: Efficient triton kernels for LLM training. *arXiv preprint arXiv:2410.10989*, 2024.
- Edward J. Hu, Yelong Shen, Phillip Wallis, Zeyuan Allen-Zhu, Yuanzhi Li, Shean Wang, Lu Wang, and Weizhu Chen. LoRA: Low-rank adaptation of large language models. In *International Conference on Learning Representations*, 2022. arXiv:2106.09685.
- Damjan Kalajdzievski. A rank stabilization scaling factor for fine-tuning with LoRA. *arXiv preprint arXiv:2312.03732*, 2023.
- Woosuk Kwon, Zhuohan Li, Siyuan Zhuang, Ying Sheng, Lianmin Zheng, Cody Hao Yu, Joseph E. Gonzalez, Hao Zhang, and Ion Stoica. Efficient memory management for large language model serving with PagedAttention. In *Proceedings of the 29th Symposium on Operating Systems Principles*, SOSP '23, pages 611–626. ACM, 2023. doi: 10.1145/3600006.3613165. arXiv:2309.06180.
- Honglin Lin, Zheng Liu, Yun Zhu, Chonghan Qin, Juekai Lin, Xiaoran Shang, Conghui He, Wentao Zhang, and Lijun Wu. MMFineReason: Closing the multimodal reasoning gap via open data-centric methods. *arXiv preprint arXiv:2601.21821*, 2026. <https://mmfinereason.github.io/>.
- Shih-Yang Liu, Chien-Yi Wang, Hongxu Yin, Pavlo Molchanov, Yu-Chiang Frank Wang, Kwang-Ting Cheng, and Min-Hung Chen. DoRA: Weight-decomposed low-rank adaptation. In *Proceedings of the 41st International Conference on Machine Learning*, volume 235 of *Proceedings of Machine Learning Research*, pages 32100–32121. PMLR, 2024. arXiv:2402.09353.

- Sourab Mangrulkar, Sylvain Gugger, Lysandre Debut, Younes Belkada, Sayak Paul, Benjamin Bossan, and Marian Tietz. PEFT: State-of-the-art parameter-efficient fine-tuning methods. <https://github.com/huggingface/peft>, 2022.
- Arjun S. Nair. Chronicals: A high-performance framework for LLM fine-tuning with 3.51x speedup over unsloth. *arXiv preprint arXiv:2601.02609*, 2026.
- Hamid Nasiri and Peter Garraghan. EDoRA: Efficient weight-decomposed low-rank adaptation via singular value decomposition. *arXiv preprint arXiv:2501.12067*, 2025.
- PyTorch. KernelAgent — multi-agent GPU kernel synthesis, 2025. URL <https://github.com/meta-pytorch/KernelAgent>.
- Samyam Rajbhandari, Jeff Rasley, Olatunji Ruwase, and Yuxiong He. ZeRO: Memory optimizations toward training trillion parameter models. In *Proceedings of the International Conference for High Performance Computing, Networking, Storage and Analysis, SC '20*. IEEE Press, 2020. doi: 10.5555/3433701.3433727. arXiv:1910.02054.
- Zhihong Shao, Peiyi Wang, Qihao Zhu, Runxin Xu, Junxiao Song, Xiao Bi, Haowei Zhang, Mingchuan Zhang, Y. K. Li, Y. Wu, and Daya Guo. DeepSeekMath: Pushing the limits of mathematical reasoning in open language models. *arXiv preprint arXiv:2402.03300*, 2024.
- Philippe Tillet, H. T. Kung, and David Cox. Triton: An intermediate language and compiler for tiled neural network computations. In *Proceedings of the 3rd ACM SIGPLAN International Workshop on Machine Learning and Programming Languages, MAPL 2019*, pages 10–19. ACM, 2019. doi: 10.1145/3315508.3329973.
- Yuze Zhao, Jintao Huang, Jinghan Hu, Xingjun Wang, Yunlin Mao, Daoze Zhang, Zeyinzi Jiang, Zhikai Wu, Baole Ai, Ang Wang, Wenmeng Zhou, and Yingda Chen. SWIFT: A scalable lightweight infrastructure for fine-tuning, 2024. URL <https://arxiv.org/abs/2408.05517>.
- Zhanda Zhu, Qidong Su, Yaoyao Ding, Kevin Song, Shang Wang, and Gennady Pekhimenko. LoRA Fusion: Efficient LoRA fine-tuning for LLMs. In *Proceedings of the Nineteenth European Conference on Computer Systems, EuroSys '26*, 2026. arXiv:2510.00206.

## A Forward Contract and Execution Semantics

### Forward Contract and Execution Semantics

#### 1. Module Interface & Compose Semantics

- **Output:** The module computes a delta  $\Delta\mathbf{Y}$ ; the caller applies  $\mathbf{Y} = \mathbf{Y}_{\text{base}} + \Delta\mathbf{Y}$ .
- **Compose Equation:**  $\Delta\mathbf{Y} = g \odot (s\mathbf{X}\mathbf{A}^\top\mathbf{B}^\top) + (g - 1) \odot \mathbf{Y}_{\text{base}}$ .

#### 2. Norm Policy

- Recomputed every forward pass; never cached across steps.
- Detached (no gradient flow), per Liu et al. [2024] §4.3.
- Accumulated in FP32 with autocast disabled.
- $\epsilon = 10^{-12}$  (fp32/fp64) or  $10^{-6}$  (bf16/fp16).
- Bias subtracted before compose, re-added after.

*Formal contract for clean-room replication.*

## B Implementation Details

**Chunk alignment.** The chunk size aligns to 64 elements on CUDA/XPU devices for Tensor Core MMA alignment on all NVIDIA architectures since Volta.

**Environment variables.** PEFT\_DORA\_FUSED (0 = force eager), PEFT\_DORA\_FUSED\_BACKWARD (1 = force fused bwd, 0 = disable, unset = auto), PEFT\_DORA\_NORM\_CHUNK\_MB and PEFT\_DORA\_FWD\_CHUNK\_MB (override 256 MB defaults).

**Scale-is-zero fast path.** When  $s = 0$ , cross and ba\_sq are skipped;  $\mathbf{U}$  and  $\mathbf{G}$  are not allocated.

**Dtype-aware epsilon.**  $10^{-12}$  for fp32/fp64;  $10^{-6}$  for bf16/fp16. For fp16 (max  $\approx 65504$ ),  $\epsilon = 10^{-6}$  limits the quotient to  $\sim 10^6$ , reducing saturation risk.

**Compose kernel autotuning.** RPP=1 is selected in 95% of autotuned entries (1149/1206). Exact config agreement between GPUs is  $\sim 9\%$ , confirming per-device autotuning is essential.

**Chunked dropout path.** When dropout is active, `_compose_with_base_chunks` iterates over output-dimension slices with adaptive sizing, decorated with `@dynamo_disable` to avoid runaway recompilations.

**Magnitude broadcast shape guard.** A shape guard gates Triton kernel dispatch on whether the magnitude vector broadcasts exclusively along the last dimension of the activation tensor. The Triton compose kernel treats magnitude as a 1-D vector along the last dimension; Conv-style shapes like  $[1, C, 1, 1]$  applied to  $[N, C, H, W]$  activations would violate this assumption. The guard checks both element count and last-dimension alignment; failing shapes route to the PyTorch fallback.

**Custom op for torch.compile.** The registered backward uses PyTorch (not Triton) because AOTAutograd traces with FakeTensors. Eager training uses Triton for both forward and backward; compiled training uses Inductor to fuse the PyTorch backward graph.

## C Kernel Specifications

This appendix provides exact specifications for the three Triton kernels and the PyTorch magnitude division stage, including casting points, fused operations, shape constraints, and reduction ordering, to support a clean-room reimplementation.

**1. Compose Forward kernel.** Fuses  $(g - 1) \odot \text{base} + g \odot s \odot \text{lora}$  in one pass. Inputs: base [bs, seq,  $d_{\text{out}}$ ], lora [bs, seq,  $d_{\text{out}}$ ],  $g$  [ $d_{\text{out}}$ ],  $s$  (scalar). Output: delta [bs, seq,  $d_{\text{out}}$ ]. All tensors in input dtype (fp16/bf16/fp32); no intermediate dtype cast.  $g$  is broadcast along all but the last dimension.

**2. Compose Backward kernel.** Fuses  $d_{\text{lora}} = g \cdot s \cdot d_{\text{out}}$  and  $d_{\text{base}} = (g - 1) \cdot d_{\text{out}}$  in a single Triton pass.  $d_{\text{mag}}$  is computed separately via a `.sum()` reduction over the batch/sequence dimensions on the inner activation; this avoids non-deterministic `tl.atomic_add` ordering.

**3. Norm Assembly kernel (norm-only).** Inputs: base\_sq [ $d_{\text{out}}$ ], cross [ $d_{\text{out}}$ ], ba\_sq [ $d_{\text{out}}$ ] (all fp32), two\_s (scalar, =  $2s$ , precomputed in fp64), s2 (scalar, =  $s^2$ , precomputed in fp64). Computes  $w_{\text{norm}} = \sqrt{\max(\text{base\_sq} + \text{two\_s} \cdot \text{cross} + \text{s2} \cdot \text{ba\_sq}, 0)}$  in fp32 with store-reload barriers after each multiply-add to prevent FMA fusion, exactly reproducing PyTorch’s separate-kernel evaluation order. The clamp preserves NaN semantics (matching `torch.clamp_min`, which propagates NaNs per IEEE 754) rather than collapsing NaNs to zero. The square root uses inline PTX `sqrt.rn.f32` for IEEE 754 correctly-rounded results (Triton’s `tl.sqrt` compiles to `sqrt.approx.ftz.f32` on SM90). The kernel returns the result in the input dtype. In default mode, it uses a fixed block size of 256 (norm kernels are launch-latency bound; see Appendix B); comprehensive autotuning over 36 configurations (block sizes 32–2048) is available for new GPU architectures. If future Triton versions change the lowering of `tl.sqrt` to IEEE-compliant rounding, the inline PTX can be removed; the Tier-3 eager fallback provides a portable alternative on any platform.

**4. Magnitude division (PyTorch).** The division  $g = \mathbf{m} / \max(w_{\text{norm}}, \varepsilon)$  is always computed in PyTorch after the norm assembly kernel returns. This ensures identical precision regardless of whether the Triton or PyTorch norm path was used, at the cost of one additional element-wise kernel launch (negligible relative to surrounding matmuls).

**Shape constraints.**  $d_{\text{out}}$  must be divisible by BLOCK\_SIZE (128). The magnitude vector must broadcast only along the last dimension of the activation; other broadcast shapes (e.g.,  $[1, C, 1, 1]$  applied to  $[N, C, H, W]$ ) route to the Tier-3 eager fallback. Non-contiguous input tensors also fall back to Tier 3.

**Tested compatibility matrix.** Table 12 summarizes the integration points explicitly tested, with notes on scope and caveats. “Tested” indicates the feature was exercised in benchmarks or convergence runs reported in this paper; “CI only” indicates coverage via the test suite (1041 tests) but not in model-level experiments.

## D Reproducibility

**Code and data.** All source code, benchmark scripts, raw JSON results, Triton autotune caches, and figure generation scripts are available at <https://github.com/socketeye44/dorafactors> (tag v1.0). The patched PEFT module is included as a git submodule (`vendor/dorafactors-peft`,

Table 12: Compatibility matrix. Scope: *Bench* = model-level benchmarks, *Conv* = convergence runs, *CI* = operator-level test suite.

Feature	Status	Scope	Notes
Mixed-precision bf16	✓	Bench+Conv	All model benchmarks and convergence runs
Mixed-precision fp16	✓	CI	Operator tests only; no model-level fp16 runs
Gradient checkpointing	✓	Bench+Conv	All model benchmarks use gradient checkpointing
ZeRO-2	✓	Conv	All convergence runs use ZeRO-2
ZeRO-3	✓	CI	Parameter gathering tested; no model-level runs
FSDP1	✓	CI	<code>summon_full_params</code> path tested
FSDP2 / DTensor	✗	—	Not supported; see §6
<code>torch.compile</code>	✓	CI	Graph-break-free when $p=0$ ; see §6
Linear layers	✓	Bench+Conv	Primary target; all benchmarks
Conv1d / Conv2d / Conv3d	✓	CI	Correctness tests; no perf benchmarks
Embedding layers	✓	CI	Formula correction (§6); no perf benchmarks

branch `v1`); cloning with `--recurse-submodules` fetches it automatically. Alternatively, the patch can be reconstructed via `git apply hf.patch` against upstream PEFT commit `20a9829`<sup>2</sup>. All commands below assume the repository root as working directory.

**Software environment.** All benchmarks were run under a single, pinned software stack: PyTorch 2.10.0+cu130 (built against CUDA 13.0 for compatibility), Triton 3.6.0, Transformers 5.2.0, CUDA toolkit 13.1 (ptxas V13.1.115), driver 580.126.09, Python 3.12.12 on Linux 6.8.0 (Ubuntu 22.04, glibc 2.35). The exact environment is published as a Docker image<sup>3</sup> for full-stack reproducibility; a `code/requirements.txt` is also included.

**Memory measurement methodology.** We report three complementary memory metrics, each appropriate to a different level of analysis:

- **Allocator peak** (`torch.cuda.max_memory_allocated()`): the maximum bytes actually allocated by PyTorch’s caching allocator. Used for microbenchmark memory deltas (Tables 1 and 7), measured after `reset_peak_memory_stats()` and `empty_cache()` to isolate a single operation’s footprint.
- **Working-set delta** (`max_memory_allocated - baseline_allocated`): the peak minus the model’s quiescent allocation, capturing the true transient overhead of DoRA’s forward/backward pass. Used for model-level gradient-computation analysis (§5.3, Table 4).
- **Reserved VRAM** (`memory_reserved`): the amount of memory the GPU physically withholds from other processes, including caching allocator fragmentation overhead. Used for peak VRAM comparison (Table 8) because it determines whether colocated workloads can share the device.

<sup>2</sup>PEFT commit: `20a9829` (v0.18.0.rc0, 2025-09-16).

<sup>3</sup>Docker image: <https://hub.docker.com/r/alexazel/dorafactors-env>. Tag: `cu131-pt210-v11m-t52-base`.

Every memory claim in this paper specifies both the metric and the dtype (fp32 vs. bf16) to avoid conflation.

### Microbenchmark reproduction.

```
# 200 repeats, extended shapes, bf16
python code/bench_dora_comprehensive.py \
  --shapes extended --repeats 200 --warmup 10 \
  --dtype bf16 --json-out results.json
```

Each run produces a self-contained JSON file with per-test timing distributions (200 samples), memory measurements, and pre-computed summary statistics. The `--shapes extended` flag generates the 20 unique activation shapes (60 entries across 3 ranks) used throughout this paper.

**Model identifiers.** All model-level benchmarks use the following Hugging Face model IDs (weights downloaded March 2026; exact file hashes in the JSON artifacts):

- Qwen/Qwen2.5-VL-32B-Instruct
- Qwen/Qwen3-VL-32B-Instruct
- Qwen/Qwen3.5-27B
- google/gemma-3-27b-it
- unsloth/Mistral-Small-3.2-24B-Instruct-2506
- Qwen/Qwen3-VL-8B-Instruct

### Convergence validation dataset.

The convergence validation (§5.9) uses a token-length-filtered subset of OpenDataArena/MMFineReason-SFT-123K-Qwen3-VL-235B-Thinking [Lin et al., 2026], repacked with mechanical field renames (`question`→`query`, `qwen3vl_235b_thinking_response`→`response`) and filtered to `tok_len ≤ 4096`. The repacked dataset is published at `eyes-ml/\protect\penalty\z@{\}MMFineReason-SFT-123K-\protect\penalty\z@{\}Qwen3-VL-235B-Thinking-QR-max4096` on Hugging Face Hub; the filtering script is included in the repository (`code/scripts/repack_mmfinereason_qr.py`).

**Convergence validation environment.** Training uses SWIFT [Zhao et al., 2024] (commit `a807cb9`) with PyTorch 2.10.0+cu130, Transformers 5.2.0, Triton 3.6.0, DeepSpeed 0.18.6, Flash-Attention 2.8.3. The full environment (including `qwen-vl-utils`, `mamba_ssm`, `flash-linear-attention`) uses the same Docker image as the benchmarks (see Software environment above) with the additional training dependencies installed.

### Model benchmark reproduction.

```
# 6 models, r=384, loss_tokens=1024
python code/bench_dora_comprehensive.py \
  --suite models --rank 384 --batch 1 --seqlen 4096 \
  --grad-accum 8 --loss-tokens 1024 --repeats 20 \
  --json-out models.json
```

**Figure regeneration.** All figures can be regenerated from the included JSON artifacts:

```
python paper/generate_figures.py
```

This produces 13 PDF figures in `paper/figures/` sourced from the `code/bench_it6/` data directory (6 GPUs × 3 dtypes for microbenchmarks, 3 GPUs for model-level). The convergence figure (Figure 12) is generated separately from TensorBoard logs via `python paper/generate_training_`

figure.py.

**Test suite.** The full test suite (1041 tests) has been validated on SM 80 through SM 120 (Ampere-Blackwell); Triton kernel tests require  $\text{SM} \geq 80$ :

```
cp code/scripts/dora.reference_hf_peft.py \
  vendor/dorafactors-peft/docs/
cd vendor/dorafactors-peft
pytest tests/test_lora_variants.py \
  tests/tuners/lora/test_dora_fused.py \
  tests/tuners/lora/test_dora_math.py -v
```

## E Full Model-Level Memory Table

Table 13 extends the main-body memory comparison (Table 8) to all six models.

Table 13: Model-level gradient-computation peak VRAM (GB) across three GPUs, all six models. Same setup as Table 8. Values from `peak_vram_mb`.

Model	Method	RTX 6000 PRO	H200	B200
Qwen2.5-VL-32B	Eager	OOM	99.2	99.2
	Fused	OOM	98.4	98.4
	Dense (B@A)	OOM	100.6	100.6
	PEFT	OOM	103.5	103.5
Qwen3-VL-32B	Eager	OOM	99.2	99.1
	Fused	OOM	98.4	98.4
	Dense (B@A)	OOM	100.5	100.4
	PEFT	OOM	103.0	102.9
Qwen3.5-27B	Eager	83.4	83.5	83.4
	Fused	83.3	83.4	83.3
	Dense (B@A)	84.3	84.4	84.3
	PEFT	85.4	85.5	85.4
Gemma3-27B	Eager	83.2	83.2	83.1
	Fused	82.9	83.0	82.9
	Dense (B@A)	84.3	84.4	84.3
	PEFT	86.1	86.1	86.1
Mistral-Sm-24B	Eager	71.6	71.7	71.6
	Fused	70.6	70.7	70.6
	Dense (B@A)	73.3	73.4	73.3
	PEFT	77.3	77.4	77.3
Qwen3-VL-8B	Eager	29.8	29.9	29.8
	Fused	29.5	29.5	29.5
	Dense (B@A)	30.1	30.2	30.1
	PEFT	30.7	30.8	30.7

## F Single-Layer E2E Decomposition

The following figures show single-layer end-to-end (E2E) speedup, which isolates the per-layer overhead but does *not* predict model-level speedup. Compose gains compound across  $\sim 500$  DoRA modules in a real model, while per-layer backward overhead is amortized, so single-layer E2E can understate the model-level benefit.

**fp32 microbenchmark summary.** Table 14 provides the fp32 rows omitted from the main-body summary (Table 9). Norm memory  $3.2\times$  in fp32 reflects the full theoretical benefit, since both paths accumulate in fp32 and the PEFT baseline also allocates fp32 temporaries.

Table 14: Geometric mean microbenchmark speedups, fp32 (all shapes, 200 repeats). Complement to Table 9.

	Compose fwd	Backward	E2E	Norm mem
L40S fp32	1.53 $\times$	1.21 $\times$	1.04 $\times$	3.2 $\times$
A100 fp32	1.64 $\times$	1.20 $\times$	1.02 $\times$	3.2 $\times$
RTX 6000 PRO fp32	1.97 $\times$	1.27 $\times$	1.06 $\times$	3.2 $\times$
H200 fp32	1.84 $\times$	1.13 $\times$	1.03 $\times$	3.2 $\times$
B200 fp32	2.35 $\times$	1.26 $\times$	1.03 $\times$	3.2 $\times$
B300 fp32	2.23 $\times$	1.21 $\times$	1.03 $\times$	3.2 $\times$

## G Framework Survey

Table 15 summarizes the DoRA norm implementation across five major fine-tuning frameworks as of February 2026. We manually inspected the DoRA-related source code in each framework’s main branch at the specified commits/versions, searching for norm computation implementations. Paths are shown relative to each framework’s source root for readability. All use the same dense-materialization algorithm; none offer a memory-efficient alternative.

Table 15: DoRA norm implementation in major fine-tuning frameworks (February 2026).

Framework	Version	File Path	Pattern
HF PEFT	20a9829	peft/tuners/lora/dora.py	<code>torch.eye</code>
torch tune	v0.5.0	modules/peft/dora.py	Same algorithm
Unsloth	2026.3.7	Disables custom kernels	Falls back to PEFT
SWIFT (ms-swift)	a807cb9	Defers to PEFT/Unsloth	No custom code
LLaMA-Factory	v0.9.3	Delegates to PEFT	No custom code
Axolotl	v0.6.0	Delegates to PEFT	No custom code

Single-Layer E2E: B200, bf16, h=4096, bs=4, seq=2048

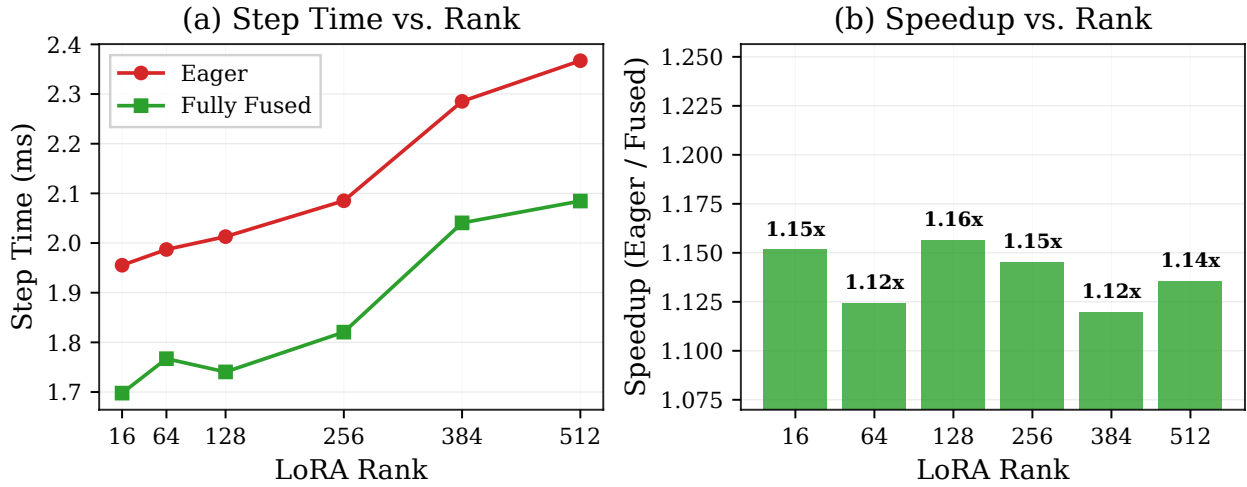


Figure 13: Single-layer E2E overhead decomposition (B200, bf16,  $d = 4096$ ,  $bs=4$ ,  $seq=2048$ ). Single-layer E2E does not predict model-level speedup: compose gains compound across  $\sim 500$  DoRA modules while per-layer backward overhead is amortized.

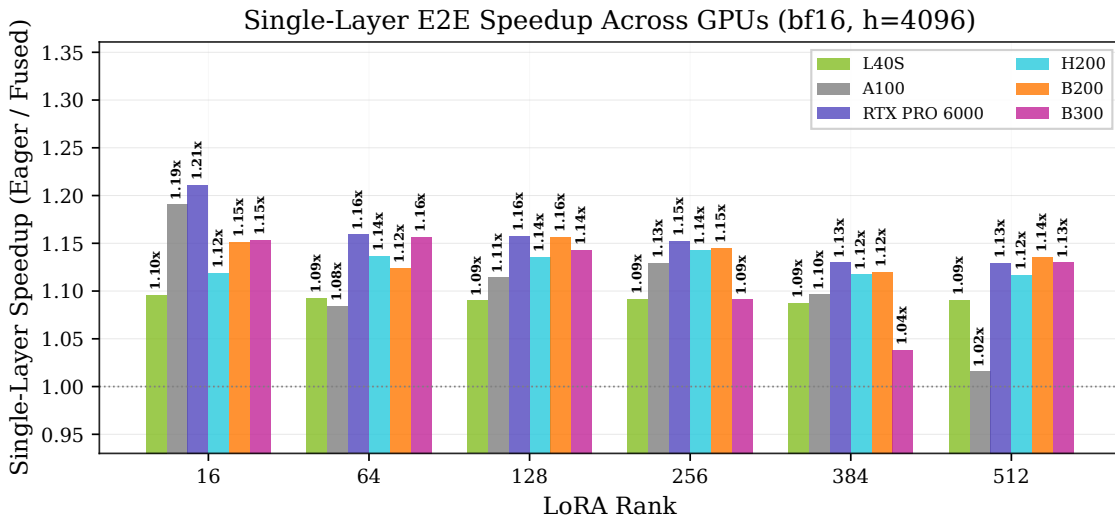


Figure 14: Single-layer E2E speedup (eager/fused) across six GPUs and ranks (bf16,  $d = 4096$ ,  $bs=4$ ,  $seq=2048$ ). All GPUs show consistent improvement.

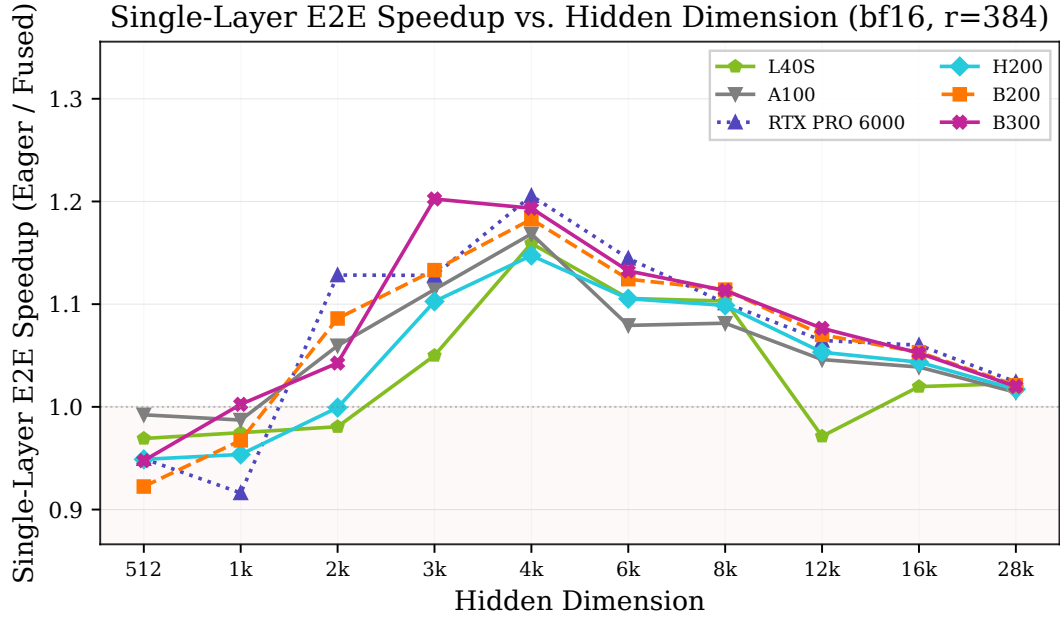


Figure 15: Single-layer E2E speedup vs. hidden dimension (bf16,  $r = 384$ , six GPUs). The benefit peaks at  $h = 3072$ – $4096$ , corresponding to common LLM sizes.